Printed in U.S.A.

64-WA/UNT-5

an ASME publication

$1.00 PER COPY
50¢ TO ASME MEMBERS

Water-Tunnel Tests of Base-Vented Torpedo Models

T. G. LANG

H. V. L. PATRICK

Hydrodynamics Group,
Research Department,
U. S. Naval Ordance Test Station,
Pasadena, Calif.

Tests were performed in a free-surface water tunnel to determine the ventilated-drag characteristics of truncated torpedo models. The streamlined, fully wetted model used for comparison in the experiments was a body of revolution with a fineness ratio of 8:1 and a diameter of 2 in. The drag based on body volume for most of the vented, truncated models was equal to the drag of the streamlined, fully wetted model. One particular model, with a short, boat-tailed afterbody, was the best of the vented configurations from the standpoint of combined low drag and low-air-flow requirement. At no time during the tests did any of the models ventilate forward of the base.

Contributed by the Underwater Technology Division for presentation at the Winter Annual Meeting, New York, N. Y., November 29-December 4, 1964, of The American Society of Mechanical Engineers. Manuscript received at ASME Headquarters, August 26, 1964.

Written discussion on this paper will be accepted up to January 10, 1965.

Copies will be available until October 1, 1965.

Water-Tunnel Tests of Base-Vented Torpedo Models

T. G. LANG H. V. L. PATRICK

NOMENCLATURE

A = cross-sectional area of torpedo ($\pi d^2/4$), sq ft
A_B = base area of torpedo ($\pi d_b^2/4$), sq ft
C_{D_A} = drag coefficient based on cross-sectional area ($D/q_\infty A$)
$C_{D_\forall}$ = drag coefficient based on volume ($D/q_\infty \forall^{2/3}$)
d = diameter of torpedo, ft
d_b = diameter of base, ft
D = drag, lb
F = Froude number $V/(g\ell)^{\frac{1}{2}}$
g = acceleration of gravity, 32.13 ft/sec^2
K = ventilation number $(P_\infty - P_c)/q_\infty$
ℓ = length of torpedo, ft
P_c = base-cavity pressure, psf
P_∞ = free-stream static pressure, psf
q_∞ = free-stream dynamic pressure ($1/2\ \rho V_\infty^2$), psf
Q = air-flow rate at free stream pressure, cfs
Q' = air-flow rate coefficient ($Q/V_\infty A_B$)
R_ℓ = Reynolds number ($V_\infty \ell/\nu$)
$\forall$ = torpedo body volume, cu ft
V_∞ = free stream velocity, fps
α = angle of attack, deg
ρ = density of the fluid, slugs/ft^3
ν = kinematic viscosity, ft^2/sec

INTRODUCTION

Interest in ventilated hydrofoils at the U. S. Naval Ordnance Test Station, Pasadena, began in the mid-1950's and resulted in several experimental and theoretical investigations (1-10).[1] A natural extension of these investigations was the study on base-vented torpedoes reported in this paper.

Since many modern torpedoes use thermal propulsion systems, exhaust gas is available for ventilation. If the drag of a torpedo with a vented, truncated tailcone is reasonably low, a considerable gain in packaging efficiency might be obtained due to the reduction in tailcone length. New possibilities for both mechanical and hydrodynamic design changes would also exist.

[1] Underlined numbers in parentheses designate References at the end of the paper.

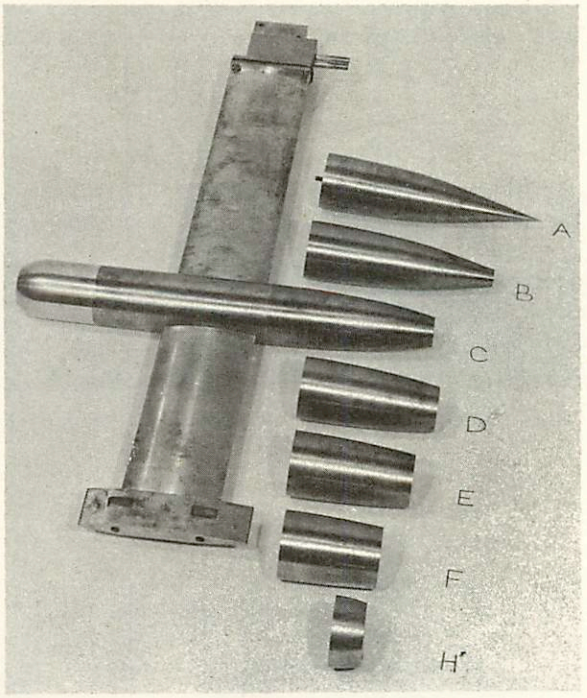

Fig. 1 Models and struts

To obtain sufficient basic data for design purposes, a series of experiments was planned at the free-surface water tunnel, California Institute of Technology (CIT). It was decided to test one streamlined model and seven base-vented models having various extents of truncation. The objective was to measure drag and cavity pressure as a function of air-flow rate, angle of attack, and tunnel speed. The results would determine:

1 Whether base-vented torpedoes have low enough drag to be feasible.

2 The magnitude of the required gas-flow rates.

3 The cavity pressures involved.

4 The restrictions imposed by speed or angle of attack.

5 Whether ventilation occurs ahead of the base.

DESCRIPTION OF MODEL AND INSTRUMENTATION

The streamlined torpedo model, designated as Model A, had a fineness ratio of 8:1, with a blunt nose faired into a 2-in-dia cylindrical center

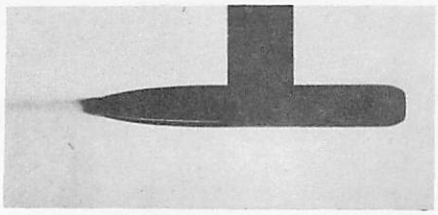

Fig. 2 Model C, partially vented

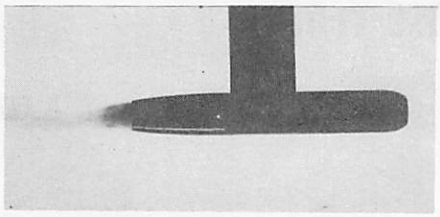

Fig. 3 Model D, partially vented

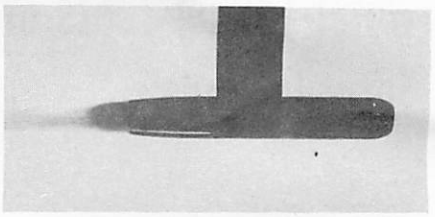

Fig. 4 Model E, partially vented

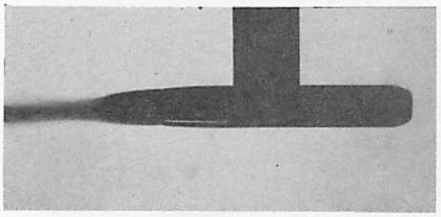

Fig. 5 Model F, partially vented

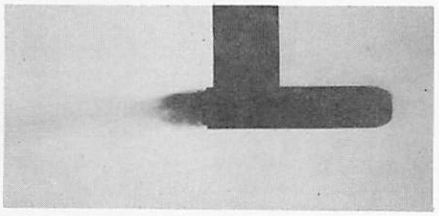

Fig. 6 Model G, partially vented

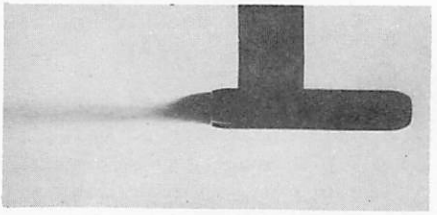

Fig. 7 Model H, partially vented

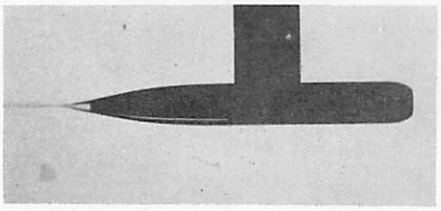

Fig. 8 Model B, base vented

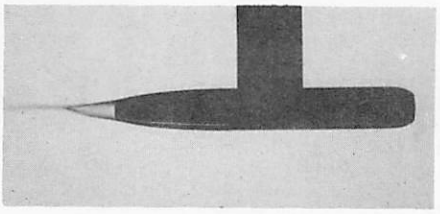

Fig. 8 Model C, base vented

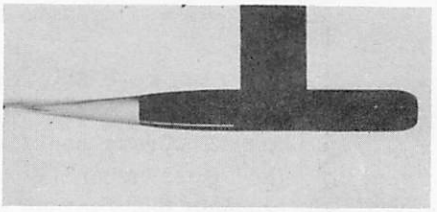

Fig. 10 Model D, base vented

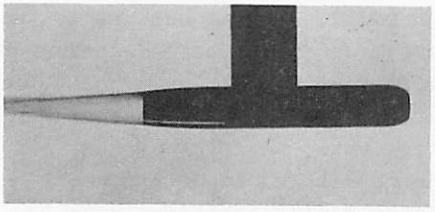

Fig. 11 Model E, base vented

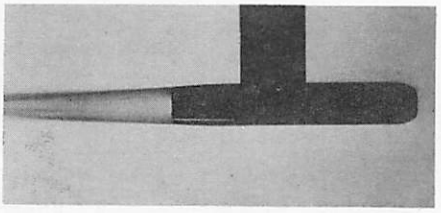

Fig. 12 Model F, base vented

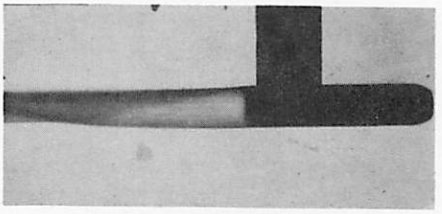

Fig. 13 Model G, base vented

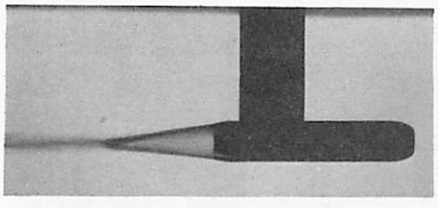

Fig. 14 Model H, base vented

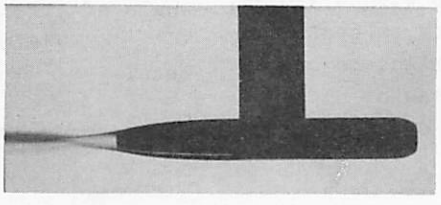

Fig. 15 Model C, base vented, high air-flow rate

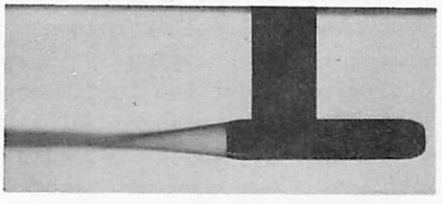

Fig. 16 Model H, base vented, high air-flow rate

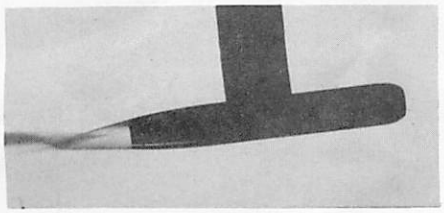

Fig. 17 Model D, base vented, side view, α = 6 deg

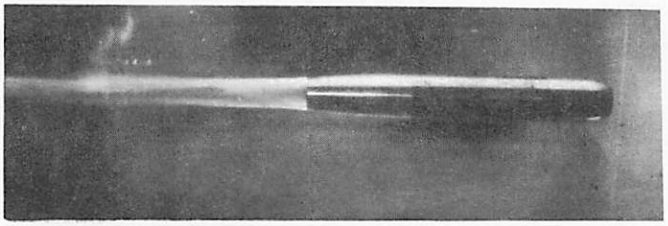

Fig. 18 Model D, base vented, bottom view, α = 6 deg

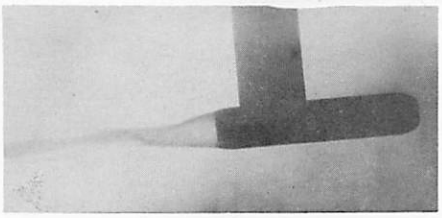

Fig. 19 Model H, base vented, side view, α = 6 deg

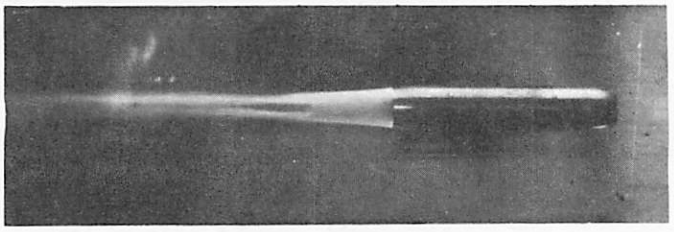

Fig. 20 Model H, base vented, bottom view, α = 6 deg

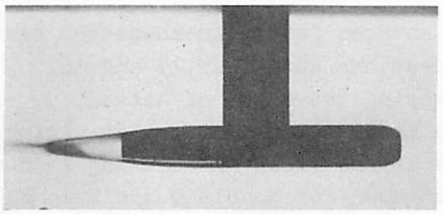

Fig. 21 Model D, early stage of cavity collapse

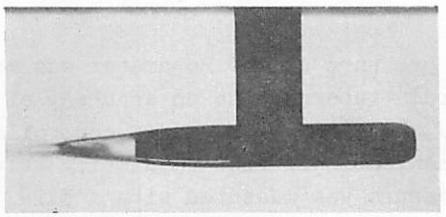

Fig. 22 Model D, later stage of cavity collapse

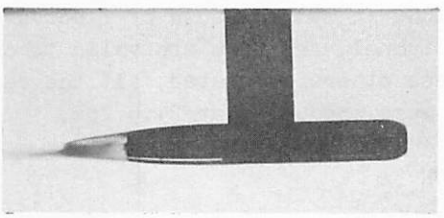

Fig. 23 Model D, still later stage of cavity collapse

section. The afterbody was the David Taylor Model Basin 4174 shape faired into a 24-deg cone. Models B-G were base-vented and were identical to Model A except that their tail cones were truncated at various diameters. Model G was simply Model A without a tail cone. Model H was also base-vented, but had a boat-tailed afterbody consisting of an arc of 3-in. radius. The basic forward section and its interchangeable afterbodies are shown in Fig.1. The models varied as follows:

Configuration	Ratio of base to cylinder diameter, percent
A	0
B	30
C	50
D	72
E	81
F	89
G	100
H	87

The models were supported with a lenticular strut 3/8 in. thick, with a chord length of 3 in. Two air channels passed through the strut, then through the model to ports in the base; one was used for measuring base-cavity pressure, while the other was used for supplying air for ventilation. The joint between the afterbody and the center section was sealed with a flat gasket to prevent air leakage.

A Fischer and Porter Company Rotameter was used for measuring the air-flow rate within 1 per-

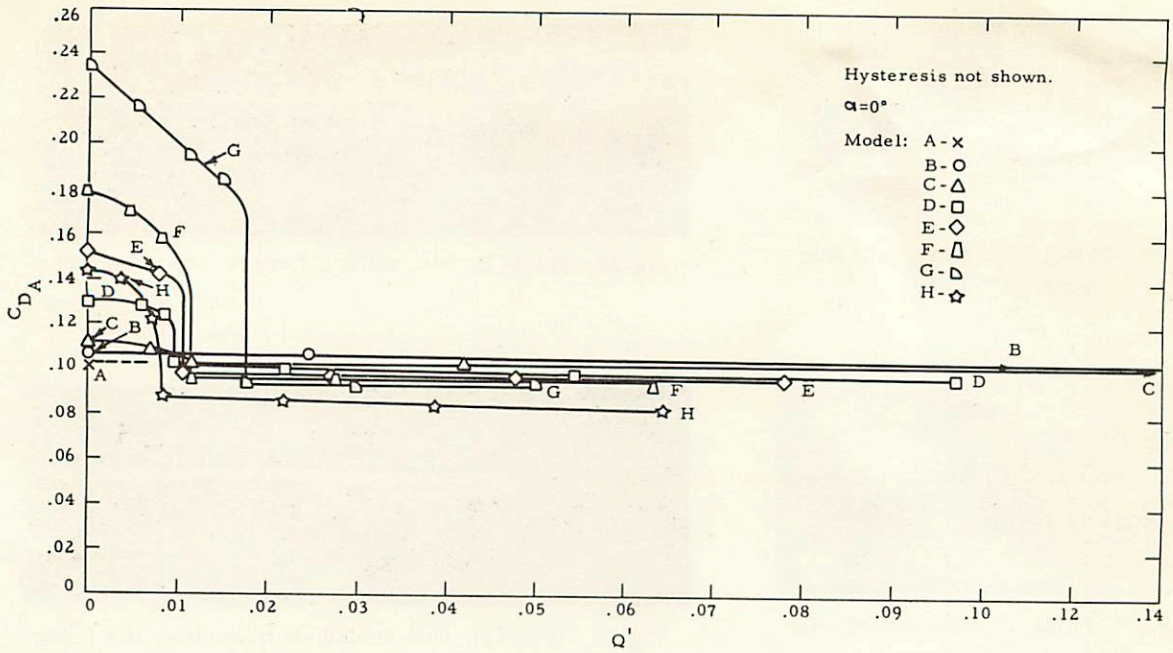

Fig. 24 C_{D_A} versus Q', Models A through H

cent. The air pressure at the Rotameter was measured by a bourdon-tube gage to an accuracy of 1/10 psi, while the air-flow rate was controlled by means of a conventional flow-regulating valve. Base-cavity pressure was measured with a CIT-developed series of water manometers and valves having an accuracy of about 2 percent.

The CIT free-surface water tunnel is described in (11), and the mechanical balance used in measuring drag in (12). The balance measures the drag to 1/1000 lb but, because of fluctuations of flow in the tunnel, the data are valid to only 1/100 lb. Unless otherwise stated, all the tests described here were conducted at 24.6 fps.

FLOW DESCRIPTION

The flow patterns behind the bases of Models C-H, when they are partially wetted, are shown in Fig.2-7. Note that a relatively short region of separated flow, composed of a bubbly water mixture, exists directly behind the bases.

As the air-flow rate increases, an increasing amount of air is mixed with the water in the region behind the base until suddenly an air-filled cavity appears. The air-flow rate at this point is called the critical value, and the model is said to be base-vented. Figs.8-14 show Models B-H with base-vented cavities. Note how the air-water interface tends to extend the streamlined body contour rearward, so that a pseudo tail cone is formed.

If the air-flow rate is further increased, the cavity changes little in shape but becomes distended near the end, Figs.15 and 16.

Increasing the angle of attack, α, of a base-vented model has the effect of making the cavity more asymmetrical and causing twin vortices to form, as shown for Models D and H in Figs.17-20

The air-flow rate can be reduced below the critical value without disturbing the air-filled cavity; this phenomenon is called a "hysteresis effect," since the critical air-flow rate with reducing flow, Q_{cr-}, is less than the critical flow rate with increasing flow, Q_{cr+}. If the flow rate is then reduced further, the air-filled cavity collapses and the original flow pattern, composed of a gas-water mixture, arises once again. The various stages of collapse can be seen in Figs. 21-23 for Model D. As the cavity gets smaller, the re-entrant jet can be seen to impinge on the lower cavity wall closer and closer to the base. When the disturbance inside the cavity caused by the reentrant jet is sufficiently great, the cavity collapses and takes on the appearance of Fig.3.

RESULTS AND ANALYSIS

The drag coefficients C_{D_A} and $C_{D_\forall}$ are plotted as functions of the dimensionless air-flow rate Q' in Fig.24 and 25, respectively, for Models A-H at $\alpha = 0^o$. Perhaps the most reasonable way to compare drag is on the basis of unit volume, as in Fig.25, rather than unit cross-sectional area, as in Fig.24. When this is done, the result is that $C_{d_\forall}$, for all base-vented models except G, is es-

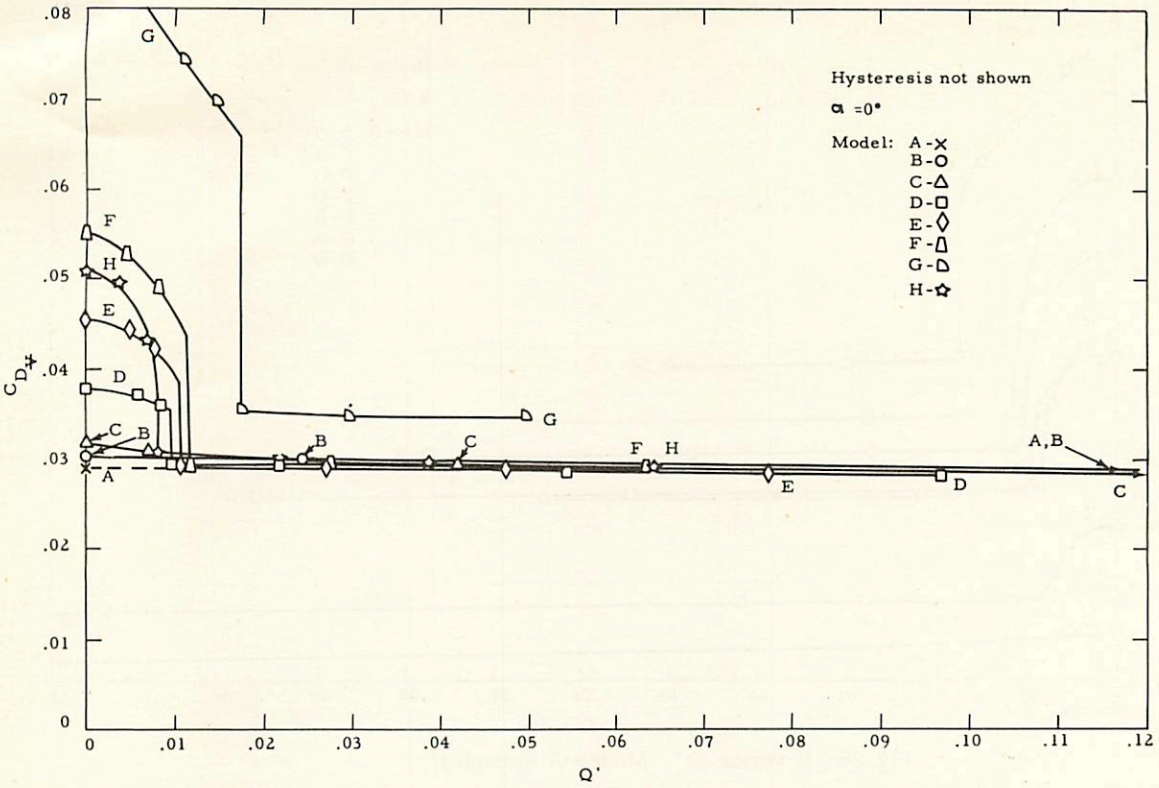

Fig. 25 $C_{D_\forall}$ versus Q', Models A through H

sentially the same as for Model A, the parent streamlined model. The exception, Model G

$$\frac{d_c}{d} = 100 \text{ percent}$$

has 25 percent higher drag.

It is seen that the fully wetted drag based on the volume of each model increases as the truncation diameter increases, with the exception of Model H (d_c/d = 87 percent), whose drag lies midway between Model E (d_c/d = 81 percent) and Model F (d_c/d = 89 percent). The primary difference between the models is that Model H has much greater curvature ahead of its base. Typical of all the curves is the sudden reduction in drag to a minimum value as Q'_{cr} is reached. The drag then remains essentially constant as Q' increases further.

CAVITY PRESSURE

Cavity pressure, expressed in dimensionless form, is represented by the ventilation number

$$K = \frac{P_\infty - P_c}{q_\infty}$$

where P_∞ and q_∞ are the free-stream static and dynamic pressures, respectively, and P_c is the cavity pressure. Looking first at the fully wetted base pressure in terms of cavity number K, it is seen in Fig.26 that K increases progressively as truncation diameter increases, except for Model H. The increased tailcone curvature of Model H has apparently produced an increase in its base pressure and a reduction in its drag.

When the models are vented, a similar progression in the increase of K with increasing truncation diameter is seen, again with the exception of Model H. The photographs of the vented

TABLE 1

Model	α, (deg)	$\frac{d_c}{d}$	Q'_{cr+}	Q'_{cr-}
B	0	30	--a	--a
C	0	50	0.007-0.011	--a
D	0	72	0.010	0.006
E	0	81	0.010	0.006
F	0	89	0.012	0.007
G	0	100	0.017	0.010
H	0	87	0.008	0.006
H	2.62	87	0.009	0.009
H	4.29	87	0.011	0.011

[a]Not measurable with the equipment used.

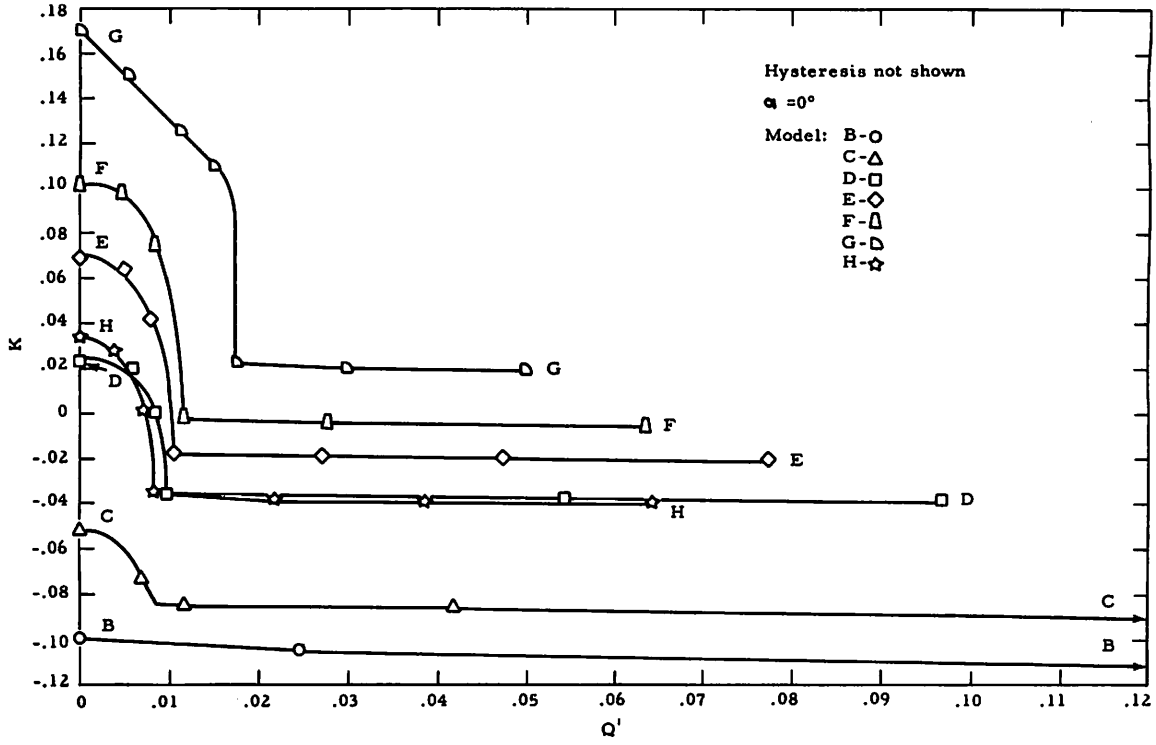

Fig. 26 K versus Q', Models A through H

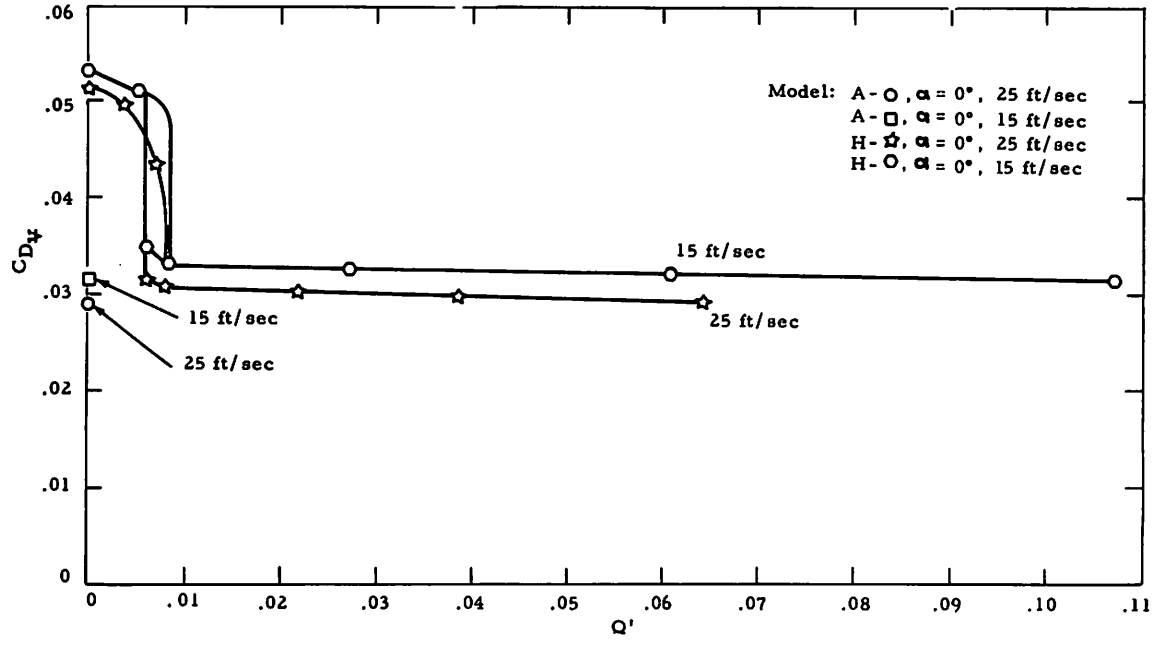

Fig. 27 Effect of tunnel speed on C_{D_V}, Models A and H

condition, Fig. 8-14 indicate that the cavity length of Model H is much shorter than those of the basic family having the same truncation diameter; this is apparently caused by the increased tailcone angle and the curvature at its base. Note that the cavity pressures of all the base-vented models are greater than the depth pressure, with the exception of Model G, the 100 percent cut-off; this result is expected, however, since any potential-flow solution of a streamlined body (i.e.,

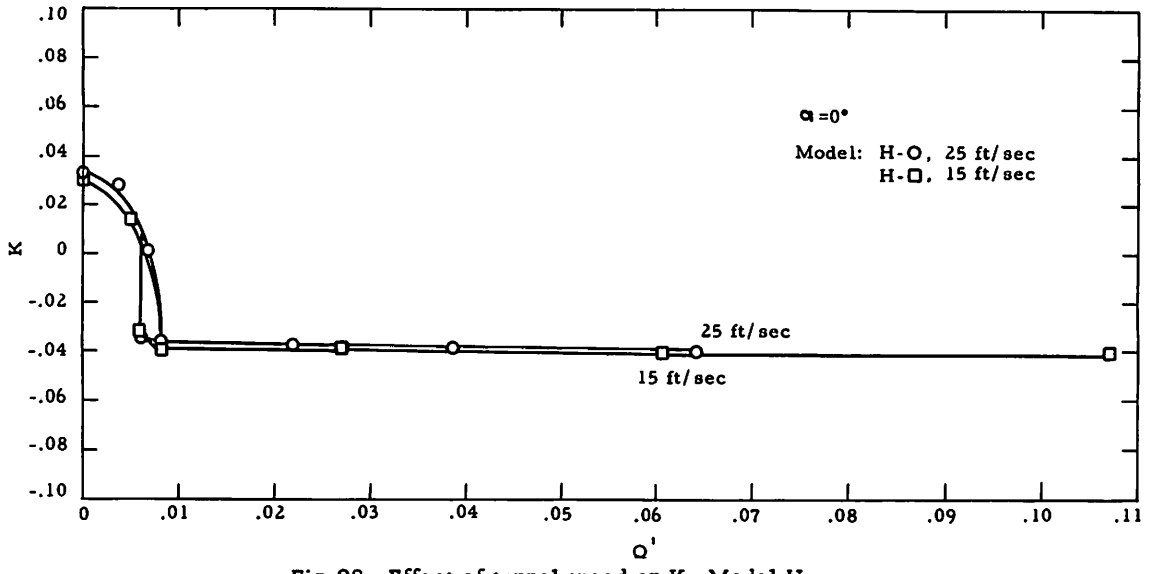

Fig. 28 Effect of tunnel speed on K, Model H

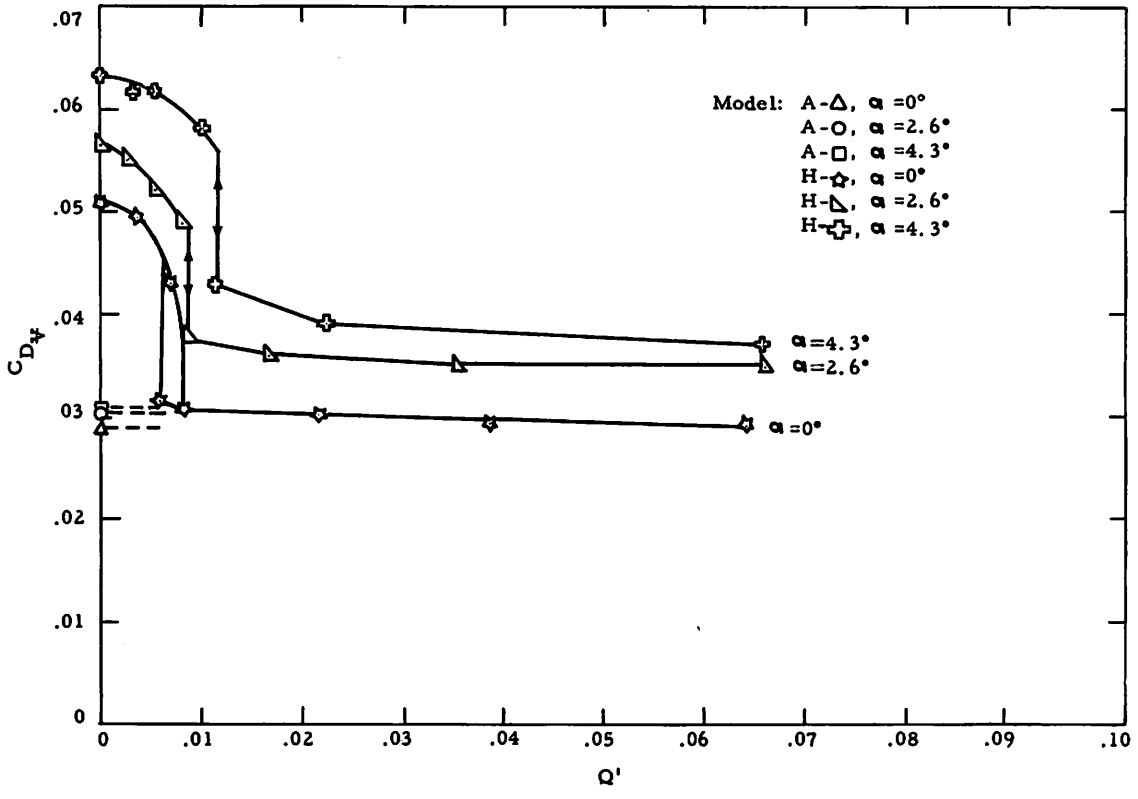

Fig. 29 Effect of angle of attack on C_{D_Ψ}, Models A and H

body plus cavity) would predict a pressure greater than free-stream at the tail.

CRITICAL AIR-FLOW RATE

It is seen in Figs.24, 25, and 26 that when the air-flow rate reaches the critical value Q'_{cr}, then C_{d_A}, C_{d_Ψ}, and K all suddenly and simultaneously reduce to steady minimum values. This phenomenon occurs simultaneously with the formation of an air-filled cavity. All the data in Figs.24, 25, and 26 were acquired by increasing the air-flow rate; the hysteresis effect caused by reducing air-flow rate is not shown. Table 1 derived

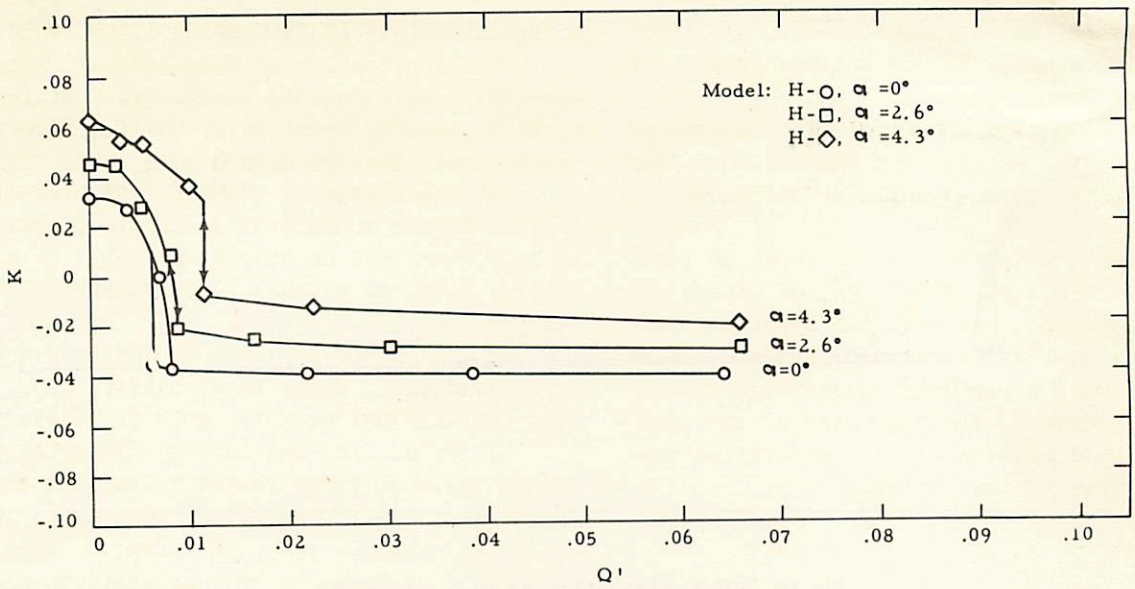

Fig. 30 Effect of angle of attack on K, Model H

from the basic data sheets shows the values of Q'_{cr+} and Q'_{cr-} as a function of model configuration, angle of attack, and truncation diameter.

It is seen that some of the critical airflow rates are very low, since Q' represents the fraction of free-stream velocity required to ventilate the base. The value of Q'_{cr} for Model H is much lower than those of the other models with equivalent truncation diameters.

EFFECT OF TUNNEL SPEED

Tests on Models A and H were conducted to determine whether significant scaling effects occurred as the result of a change in tunnel velocity. The results in Fig.27 show that the ratio of C_{d_V} at 15 fps to C_{d_V} at 25 fps for models A and H are 1.09 and 1.07, respectively. The ratio of turbulent skin-friction coefficients at the two Reynolds numbers is about 1.08. Consequently, the change in measured drag appears to be caused by the change in frictional drag with Reynolds number.

It is also seen in Fig.27 that a change in speed has no effect on either Q'_{cr+} or Q'_{cr-}. Similarly, speed has no effect on cavity number, K, as plotted in Fig.28. As a result, the cavity characteristics appear to be functions of dynamic pressure and not Froude number or Reynolds number.

ANGLE OF ATTACK

The effect of angle of attack on C_{D_V} (Models A and H) and K (Model H) are shown in Figs. 29 and 30, respectively. The drag of Model H increased about 30 percent from $\alpha = 0^o$ to $\alpha = 4.3^o$ and the drag of Model A increased 7 percent. The drag increase of Model H was believed to have resulted from a reduction in base pressure caused by an increased asymmetry of the cavity and the formation of twin vortices. The value of K is seen to increase, i.e., base pressure reduces, from -0.036 at $\alpha = 0^o$ to -0.006 at $\alpha = 4.3^o$.

It is also seen in Figs.29 and 30 that Q'_{cr+} increases from 0.008 to about 0.011 as α increases from 0^o to 4.3^o. The hysteresis effect disappears above $\alpha = 2.6^o$.

CONCLUSIONS

The results show that there was no drag penalty for most of the base-vented configurations since the drags based on body volume were the same as for the fully wetted streamlined configuration. Of all the configurations tested, only the model with the 100 percent truncation had a higher drag per unit volume than the streamlined model.

The boat-tailed configuration Model H had the shortest tail cone and the lowest critical airflow rate of all the configurations tested, with no penalty in drag.

It was found that the cavity pressure was greater than the depth pressure for all base-vented models having a truncation diameter less than about 90 percent. The gas-flow hysteresis effect was found to increase with increasing truncation diameter and to reduce with increasing angle of attack.

The results show that the drag coefficient varies with Reynolds number in proportion to the coefficient of turbulent skin friction. Neither

the critical air-flow-rate coefficient, Q'_{cr} nor the ventilation number, K, was noticeably affected by Reynolds or Froude numbers.

There was no sign of ventilation forward of the base during the entire test series, including exploratory tests up to an angle of attack of 6 deg.

There was a drag increase of about 30 percent for Model H placed at an angle of attack of 4.3 deg; in addition, the critical air-flow coefficient, Q'_{cr}, increased about 36 percent. These two increases were apparently caused by a reduction in base pressure, the asymmetry of the base cavity, and the formation of twin gas-filled vortices at the rear of the cavity.

ACKNOWLEDGMENT

The authors wish to acknowledge the help of Mr. Ted Bate of the CIT Hydrodynamics Laboratory for setting up the instrumentation, calibrating the balance, and aiding the authors in taking data. The authors also wish to thank Mr. H. T. Yerby of NOTS and Mr. T. Kiceniuk of CIT for technically reviewing this report. The work was performed under Bureau of Naval Weapons Task Assignment RUTO-3E-000/216 1/R009-01-03 under the cognizance of Task Engineer, H. Eggers.

REFERENCES

1 U. S. Naval Ordnance Test Station. "Base-Vented Hydrofoils," by T. G. Lang, China Lake, Calif., NOTS, 19 October 1959 (NAVORD REPORT 6606, NOTS TP 2346).

2 "Theoretical Lift and Drag on Vented Hydrofoils for Zero Cavity Number and Steady Two-Dimensional Flow," by A. G. Fabula, China Lake, Calif., NOTS, 4 November 1959 (NAVORD REPORT 7005, NOTS TP 2360).

3 "Water-Tunnel Tests of Hydrofoils With Forced Ventilation," by T. G. Lang, Dorothy A. Daybell, and K. E. Smith, China Lake, Calif., NOTS, 10 November 1959 (NAVORD REPORT 7008, NOTS TP 2363).

4 "Application of Thin-Airfoil Theory to Hydrofoils With Cut-Off Ventilated Trailing Edge," by A. G. Fabula, China Lake, Calif., NOTS, 13 September 1960 (NAVWEPS REPORT 7571, NOTS TP 2547).

5 "Water-Tunnel Tests of a Base-Vented Hydrofoil Having a Cambered Parabolic Cross Section," by T. G. Lang and Dorothy A. Daybell, China Lake, Calif., NOTS, 10 October 1960 (NAVWEPS REPORT 7584, NOTS TP 2569).

6 "Linearized Theory of Vented Hydrofoils," by A. G. Fabula, China Lake, Calif., NOTS, 7 March 1961 (NAVWEPS REPORT 7637, NOTS TP 2650).

7 T. G. Lang and Dorothy A. Daybell, "Water Tunnel Tests of Three Vented Hydrofoils in Two-Dimensional Flow," Journal of Ship Research, vol. 5, no. 3, December 1961, pp. 1-15.

8 A. G. Fabula, "Thin-Airfoil Theory Applied to Hydrofoils With a Single Finite Cavity and Arbitrary Free-Streamline Detachment," Journal of Fluid Mechanics, vol. 12, part 2, 1962, pp. 227-240.

9 U. S. Naval Ordnance Test Station. "Free-Surface Water-Tunnel Tests of an Uncambered Base-Vented Parabolic Hydrofoil of Aspect Ratio One," by T. G. Lang and Dorothy A. Daybell, China Lake, Calif., NOTS, September 1962 (NAVWEPS REPORT 7920, NOTS TP 2942).

10 "Comparison of Theory and Experiment for Vented Hydrofoils," by A. G. Fabula, China Lake, Calif., NOTS, March 1963 (NAVWEPS REPORT 7941, Part 2; NOTS TP 3066).

11 T. T. Knapp, J. Levy, J. P. O'Neill and F. B. Brown, "The Hydrodynamics Laboratory of the California Institute of Technology," Trans. ASME, vol. 70, no. 5, July 1948, pp. 437-57.

12 California Institute of Technology, "An Experimental Study of the Hydrodynamic Forces Acting on a Family of Cavity Producing Conical Bodies of Revolution Inclines to the Flow," by Taras Kiceniuk, Pasadena, Calif., CIT, June 1954, CIT Hydrodynamics Laboratory Report E-12. 17.